

Cite this: *Nanoscale*, 2012, **4**, 1695

www.rsc.org/nanoscale

PAPER

## Binary ionic porphyrin nanosheets: electronic and light-harvesting properties regulated by crystal structure†

Yongming Tian,<sup>ab</sup> Christine M. Beavers,<sup>c</sup> Tito Busani,<sup>de</sup> Kathleen E. Martin,<sup>ae</sup> John L. Jacobsen,<sup>f</sup> Brandon Q. Mercado,<sup>f</sup> Brian S. Swartzentruber,<sup>a</sup> Frank van Swol,<sup>ae</sup> Craig J. Medforth<sup>eg</sup> and John A. Shelnutt<sup>\*ah</sup>

Received 22nd November 2011, Accepted 10th January 2012

DOI: 10.1039/c2nr11826b

Crystalline solids self-assembled from anionic and cationic porphyrins provide a new class of multifunctional optoelectronic micro- and nanomaterials. A 1 : 1 combination of zinc(II) tetra(4-sulfonatophenyl)porphyrin (ZnTPPS) and tin(IV) tetra(*N*-methyl-4-pyridiniumyl)porphyrin (SnTNMePyP) gives porphyrin nanosheets with high aspect ratios and varying thickness. The room temperature preparation of the nanosheets has provided the first X-ray crystal structure of a cooperative binary ionic (CBI) solid. The unit cell contains one and one-half molecules of aquo-ZnTPPS<sup>4-</sup> (an electron donor) and three half molecules of dihydroxy-SnTNMePyP<sup>4+</sup> (an electron acceptor). Charge balance in the solid is reached without any non-porphyrinic ions, as previously determined for other CBI nanomaterials by non-crystallographic means. The crystal structure reveals a complicated molecular arrangement with slipped  $\pi$ - $\pi$  stacking only occurring in isolated dimers of one of the symmetrically unique zinc porphyrins. Consistent with the crystal structure, UV-visible J-aggregate bands indicative of exciton delocalization and extended  $\pi$ - $\pi$  stacking are not observed. XRD measurements show that the structure of the Zn/Sn nanosheets is distinct from that of Zn/Sn four-leaf clover-like CBI solids reported previously. In contrast with the Zn/Sn clovers that do exhibit J-aggregate bands and are photoconductive, the nanosheets are not photoconductive. Even so, the nanosheets act as light-harvesting structures in an artificial photosynthesis system capable of reducing water to hydrogen but not as efficiently as the Zn/Sn clovers.

### Introduction

New highly-absorbing and stable optoelectronic materials are of intense interest especially for the development of renewable and sustainable energy sources.<sup>1-6</sup> Crystalline solids composed of two or more different light-absorbing molecules are of particular interest because they possess myriad advantageous photo-physical and photochemical processes that can be exploited.

Recently, we described a novel class of nano- and microscale organic optoelectronic solids synthesized by ionic self-assembly of oppositely charged porphyrin ions.<sup>7-12</sup> Because of the potential for cooperative interactions between the two types of porphyrins (*e.g.*, electron donors and acceptors) these versatile and tunable materials are described as Cooperative Binary Ionic (CBI) solids.

The properties of CBI materials are expected to depend on factors such as the functionality of the individual porphyrin

<sup>a</sup>Advanced Materials Laboratory and Center for Integrated Nanotechnologies, Sandia National Laboratories, Albuquerque, NM, 87106, United States. E-mail: jasheln@unm.edu; Fax: +505-272-7077; Tel: +505-306-8472

<sup>b</sup>Department of Materials Engineering, New Mexico Institute of Mining and Technology, Socorro, NM, 87801, United States

<sup>c</sup>Advanced Light Source, Lawrence Berkeley National Laboratory, One Cyclotron Road, Berkeley, CA, 94720, United States

<sup>d</sup>Universidade Nova de Lisboa at CENIMAT/IN, Departamento de Ciência dos Materiais, Faculdade de Ciências e Tecnologia, CEMOP-UNINOVA, 2829-516 Caparica, Portugal

<sup>e</sup>Departments of Electrical and Computer Engineering, and Chemical and Nuclear Engineering, University of New Mexico, Albuquerque, NM, 87106, United States

<sup>f</sup>Department of Chemistry, University of California, Davis, CA, 95616, United States

<sup>g</sup>REQUIMTE/Departamento de Química e Bioquímica, Faculdade de Ciências, Universidade do Porto, 4169-007 Porto, Portugal

<sup>h</sup>Department of Chemistry, University of Georgia, Athens, GA, 30602, United States

† Electronic supplementary information (ESI) available: Details of the crystallographic refinement, tables of refinement parameters and bond distances and NSD analysis, and figures showing SEM images of Zn/Sn nanosheets and clovers, the solid grown at different porphyrin concentrations, SEM images of nanosheets at high and low magnification, an ORTEP image showing the five crystallographically distinct porphyrin molecules and the water molecules, and a view of the crystal structure down the *b* axis are given in the ESI. CCDC reference number 833006. For ESI and crystallographic data in CIF or other electronic format see DOI: 10.1039/c2nr11826b

molecules and their order and spatial arrangement within the ionic solid. The latter influences the cooperative interactions between adjacent molecules and properties such as electron transfer as well as their interactions over longer distances, which influence collective properties such as conductivity. A unique feature of the porphyrin CBI solids synthesized to date<sup>7–13</sup> is that the metals in the porphyrin anions and cations can be selected based on the desired physical and chemical properties without significantly altering their crystalline structure as determined from XRD powder patterns.<sup>8</sup> This allows the functional properties of the porphyrin molecules to be altered and tuned systematically without changing their spatial arrangement. However, detailed knowledge of the internal structures and intermolecular interactions, and the relationship of these structural features to function, is currently lacking for the CBI solids as no X-ray crystal structure determinations have been reported.

Herein, we report the synthesis of nanosheets by the ionic self-assembly of Zn tetra(sulfonatophenyl)porphyrin (ZnTPPS<sup>4-</sup>) and Sn tetra(*N*-methyl-4-pyridiniumyl)porphyrin (SnTNMePyP<sup>4+</sup>), shown in Fig. 1a and 1b, respectively, and the first crystal structure of a CBI solid. The nanosheets have high aspect ratios and are of varying thickness (See Fig. 2). Despite the nanoscale thickness of most of the sheets, a crystal suitable for X-ray crystallography using the Advanced Light Source synchrotron was found and the X-ray structure determined. We demonstrate that electronic properties of the nanosheets ascertained by conducting atomic force microscopy (AFM) can be rationalized based on the crystal structure. The nanosheets are also characterized by SEM, XRD, and UV-visible spectroscopy. Finally, we show that the Zn/Sn nanosheets can be utilized as light-harvesting structures for the generation of H<sub>2</sub> in the presence of sacrificial electron donor, electron relay, and platinum nanocatalyst photocatalytically generated by the nanosheets.

## Experimental section

ZnTPPS and SnTNMePyP were obtained from Frontier Scientific and their purity was confirmed by proton NMR spectroscopy. Potassium tetrachloroplatinate(II) (K<sub>2</sub>PtCl<sub>4</sub>; 99.99%), L-ascorbic acid (99+%), triethanolamine (99+%), and methylviologen (MV) were purchased from Aldrich and used without further purification. All the solutions used in the syntheses were prepared using ultrapure water from a Barnstead Nanopure water system and were filtered through 0.2- $\mu$ m syringe filters.

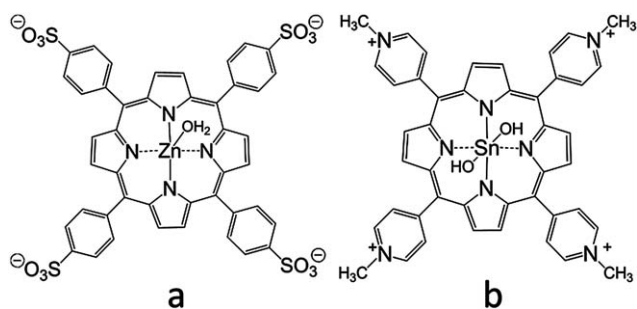


**Fig. 1** Zn(II) tetrakis(4-sulfonatophenyl)porphyrin<sup>4-</sup> (a) and Sn(OH)<sub>2</sub> tetra(*N*-methyl-4-pyridiniumyl)porphyrin<sup>4+</sup> (b) used in the synthesis of the nanosheets and other structures shown in Fig. 2.

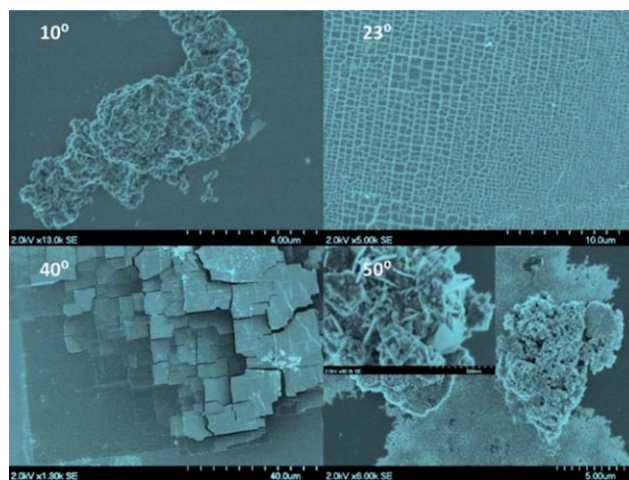


**Fig. 2** SEM images of the Zn/Sn structures obtained by ionic self-assembly of the porphyrins shown in Fig. 1 at different temperatures.

The nanosheets and other materials shown in Fig. 2 were prepared by taking 1 mL aliquots of 210  $\mu$ M solutions of ZnTPPS and SnTNMePyP equilibrated at the desired temperatures, mixing the solutions, and allowing the reaction vessel to sit undisturbed at that temperature for 12 h.

For the platinization reaction, aqueous K<sub>2</sub>PtCl<sub>4</sub> solution (20 mM) was prepared and equilibrated overnight, and ascorbic acid solution (0.2 M) was freshly prepared before each reaction. For photocatalytic self-platinization, 6 mL of the suspension of purified Zn/Sn nanosheets grown at 23 °C (105  $\mu$ M in each porphyrin) was placed in a 20-mL glass vial and diluted with water to 10 mL. To this mixture, 150  $\mu$ L of the aged K<sub>2</sub>PtCl<sub>4</sub> solution (20 mM) and 150  $\mu$ L of ascorbic acid solution (0.2 M) were added. The Zn/Sn nanosheet mixtures were irradiated with light (0.1 W cm<sup>-2</sup> measured at the outer wall of the vessel using a Coherent Model 201 bolometer) from a projector with an incandescent lamp (ENX, 3M) for 70 min.

For the hydrogen evolution reactions, suspensions of the platinized nanosheets (6 mL) were first centrifuged to isolate the nanostructures. The precipitate was then re-dispersed in 10 mL of aqueous triethanolamine (200 mM) at pH 3 in a 25 mL glass vial generating a suspension with a concentration of 63  $\mu$ M of each porphyrin. MV was added (20 mM) and the glass vial sealed with a rubber septum, purged with argon for 10 min, and irradiated with a tungsten light source (ENX, 3M; 0.1 W cm<sup>-2</sup>). The nanosheets were kept suspended during the reaction using a magnetic stirrer bar. Gas samples (50–100  $\mu$ L) were taken from the 15 mL head space of the glass vial at time intervals (typically 24 h). The H<sub>2</sub> content was determined using a gas chromatograph (HP 5890 Series II) equipped with a 5- $\text{Å}$  molecular sieve column and a thermal conductivity detector. The carrier gas was argon. The gas chromatograph was calibrated using argon with a known concentration of hydrogen (0.492%).

Samples of the nanomaterials for XRD were prepared by depositing drops of the suspensions onto glass slides or Si wafers and air drying the samples. XRD patterns were recorded on a Siemens D500 diffractometer using Ni-filtered Cu-K $\alpha$  radiation ( $\lambda = 1.5418 \text{ \AA}$ ) in  $\theta$ - $2\theta$  scanning mode using a step size of 0.05° and a 90-second step time.

Samples for scanning electron microscopy imaging were prepared by pipetting 50  $\mu\text{L}$  of the precipitate onto Si wafers. After allowing precipitation for 2 min, excess solvent was wicked away using a Kimwipe tissue and the wafer was allowed to air dry. SEM imaging was performed on a Hitachi S-5200 Nano scanning electron microscope operating at 2 keV. Additional SEM images of Zn/Sn nanomaterials comparing the clovers and nanosheets prepared under the same experimental conditions, other morphologies of nanomaterials obtained from mixing the two porphyrins in Fig. 1 at 23  $^{\circ}\text{C}$  with different initial concentrations, and images of the 23 $^{\circ}$  nanosheets at high magnification can be found in the ESI.†

## Results and discussion

Our previous studies of CBI solids<sup>8,9</sup> produced complex dendritic microscale structures by mixing equimolar solutions of Zn(II) or Sn(IV) complexes of TPPS<sup>4-</sup> and a porphyrin cation, tetra(*N*-hydroxyethyl-4-pyridiniumyl)porphyrin (TNEtOHPyP<sup>4+</sup>), that is structurally related to the porphyrin shown in Fig. 1b. Ionic self-assembly of all four combinations of these porphyrins (Sn/Zn, Zn/Sn, Sn/Sn and Zn/Zn) was found to produce CBI solids with the expected 1 : 1 ratio of the porphyrins and similar morphologies, dimensions, and internal packing arrangements (as demonstrated by XRD studies).<sup>8</sup> However, to date these four-leaf clover-like structures (see Fig. S1a of the ESI†) have not provided suitable crystals for X-ray structure determinations.

In contrast, ionic self-assembly of the porphyrins shown in Fig. 1 under certain growth temperatures and porphyrin concentrations produced a new CBI solid in the form of nanosheets and also produced a crystal suitable for X-ray crystallography. SEM images show that the nanosheets are formed over a narrow range of temperatures (Fig. 2 [23 $^{\circ}$  and 40  $^{\circ}\text{C}$ ], Fig. S1b, and Fig. S3) and concentrations (see Fig. S2 [210  $\mu\text{M}$ ]). The nanosheets that gave the crystal used for X-ray structure determination were prepared at 23  $^{\circ}\text{C}$  by simply mixing 210  $\mu\text{M}$  solutions of the two porphyrins at a final pH of 6.75. When dry, the room-temperature nanosheets show a characteristic rectangular drying pattern (see Fig. 2 [23 $^{\circ}$ ]) that is likely not present in the air-dried crystals used for the X-ray structure determination. In suspensions, specular reflections from the flat surfaces of the rotating sheets make them look like glitter.

The many sharp reflections observed in the XRD patterns of the Zn/Sn nanosheets (Fig. 3) show them to be much more crystalline than the Zn/Sn clovers investigated previously.<sup>8,9</sup> The diffraction patterns are also distinct indicating different crystal structures for the two materials. It was shown previously that the crystal structure of the clovers was insensitive to the metals in the porphyrin rings, *i.e.*, Zn/Zn, Sn/Sn, Sn/Zn, and Zn/Sn (TPPS/TNEtOHPyP). On the other hand, changing the pyridine nitrogen substituent from ethanol (clovers) to methyl (nanosheets) is sufficient to alter the crystalline structure and morphology, presumably by modulating the steric and hydrogen bonding properties of the cationic porphyrin.

A dark red plate was found in the suspension of the 23  $^{\circ}\text{C}$  Zn/Sn nanosheets which was suitable for X-ray structure determination using synchrotron radiation. (Details are provided in the text and Tables S1 and S2 of the ESI.†) Refinement of the structure gives an asymmetric unit cell containing one complete

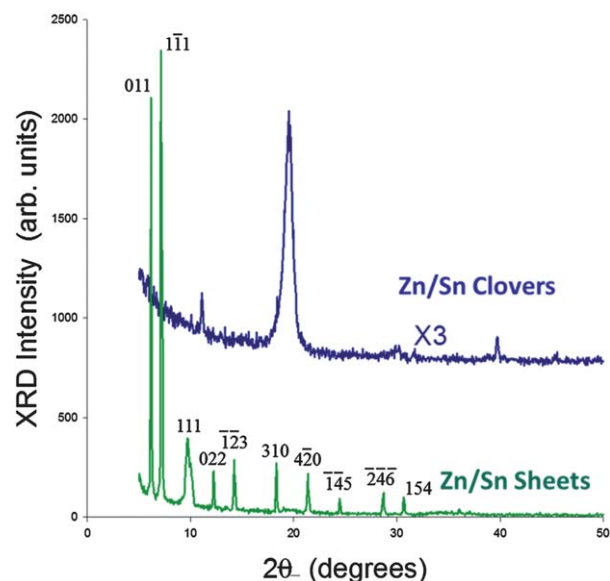


**Fig. 3** XRD diffraction patterns for the Zn/Sn nanosheets and the Zn/Sn clovers. The clover structures result from the replacement of SnTNMePyP used in the nanosheets with SnTNEtOHPyP. The sample was carefully tilted to remove most of the peaks of the Si substrate such as the peak at 69 $^{\circ}$  (not shown). Tilting does not modify the XRD pattern of the CBI solids. The nanosheets pattern was indexed using PowderCell software and the atomic positions of the Sn and Zn atoms.

Zn(H<sub>2</sub>O)TPPS<sup>4-</sup> molecule and half of a second Zn(H<sub>2</sub>O)TPPS<sup>4-</sup> molecule; the unit cell also contains three half molecules of Sn(OH<sup>-</sup>)<sub>2</sub>TNMePyP thus balancing the charge without other non-porphyrinic ions.

The porphyrin macrocycles are nearly planar except for one of the five-coordinate ZnTPPS molecules (Fig. 4a), which has a dominant saddle deformation [1.17  $\text{\AA}$ , as determined by normal coordinate structure decomposition (NSD) analysis]<sup>14,15</sup> with significant contributions from ruffling (0.26  $\text{\AA}$ ) and  $\gamma$ -waving (0.14  $\text{\AA}$ ) deformations. (The complete NSD results are given in Table S3.) The unit cell also contains 20.41 water molecules in 47 positions, all partially occupied (see Fig. S4).

There is considerable disorder in the crystal both in the water molecules and the porphyrins. The hydrogens of the water molecules were located only for the aquo axial ligand of one of the ZnTPPS<sup>4-</sup> molecules and the two water molecules adjacent to the axial ligand and hydrogen bonded to it (Fig. 4a). These were also the waters with the highest occupancy. No other hydrogens of water could be located in the density map, including on the axial ligand of the other ZnTPPS<sup>4-</sup> molecule and the hydroxides of the SnTNMePyP molecules. The structural disorder and low occupancy of the water molecules is consistent with the drying behavior noted for the porphyrin nanosheets and other crystal structures of porphyrin ions.<sup>16–21</sup> Further details of the X-ray structure methods, refinement procedure (Table S1), and bond distances (Table S2) are given in the ESI.† Fig. 4b shows the molecular packing from a view down the *a*-axis (a view down the *b* axis is shown in Fig. S5.) The water molecules (not shown) lie primarily in the sparse middle row of only SnTNMePyP molecules. There are two types of SnTNMePyP molecules in this sparse layer—one type (middle porphyrin) electrostatically

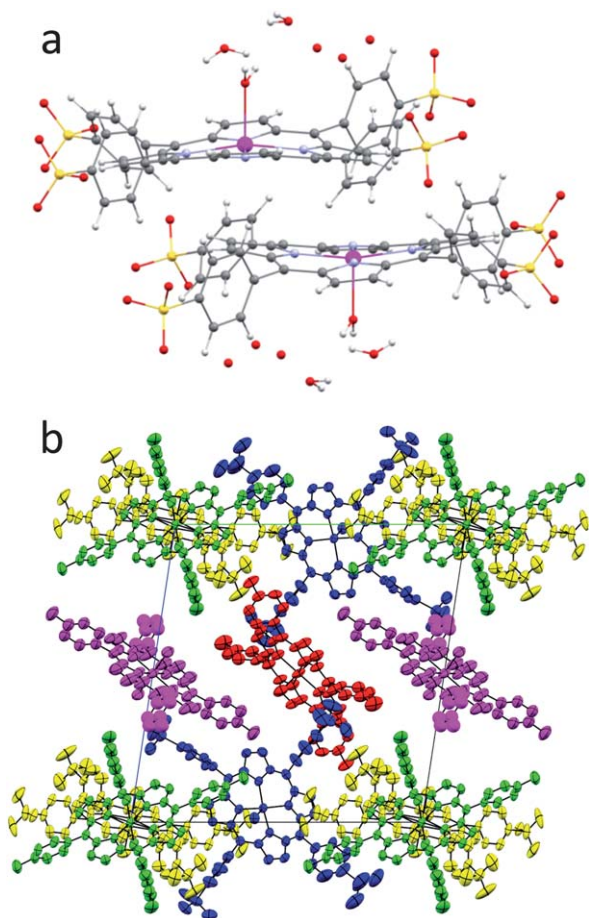


**Fig. 4** (a) The  $\pi$ - $\pi$  dimer of  $\text{Zn}(\text{H}_2\text{O})\text{TPPS}$  molecules in the crystal with associated waters, and (b) the molecular packing in the Zn/Sn nanosheet crystal as viewed down the  $a$  axis with the  $b$  axis to the right. Zn1 in blue (dimer), Zn2 in yellow, Sn1 in green, Sn2 in red, and Sn3 in magenta. Zn2 and its water ligand are disordered over an inversion center, with the Zn and axial water split into two sites above and below the porphyrin plane. Disordered water oxygen atoms are omitted for clarity. A larger ORTEP image showing the unit cell and the associated water molecules is given in Fig. S4.

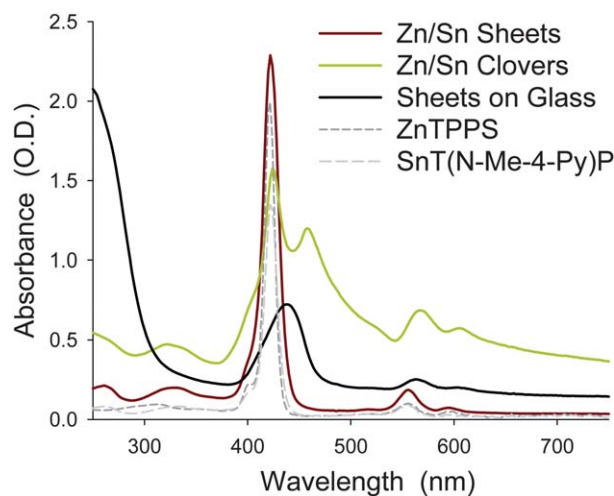
interacts strongly with ZnTPPS molecules in the adjacent layers (top and bottom), *i.e.*, the oppositely charged groups are close together. The other type (1st and 3rd porphyrins) has its N-methyl pyridinium groups farther from and interacting more non-specifically with the sulfonate groups of molecules in the adjacent layers. There are reported crystal structures of ionic porphyrins although they mostly contain only one type of porphyrin with non-porphyrin counterions.<sup>16-22</sup> The closest structures to the CBI solids are those with large calixarene counterions, but the calixarene is not photoactive and its properties are likely not easily tuned without influencing the crystal structure. A hypothetical crystal structure of a 1 : 1 mixed porphyrin CBI crystal was postulated by Hikal and Harmon based on the cell dimensions obtained from XRD.<sup>13</sup> However, the crystal structure of the nanosheets shows that more complex arrangements of the porphyrin molecules and water must be considered in CBI solids.

The nanosheet crystal structure does not reveal significant porphyrin  $\pi$ - $\pi$  stacking that could lead to strong coupling of

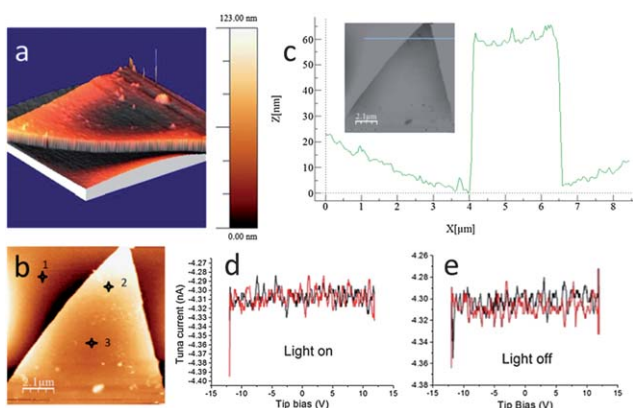
transition dipoles associated with strongly red shifted J-aggregate UV-visible absorption bands and conductivity or photoconductivity. The only  $\pi$ - $\pi$  stacking of porphyrins evident in the crystal structure is in the  $\pi$ - $\pi$  dimers formed by the ZnTPPS molecules illustrated in Fig. 4a. These dimers are widely separated in the crystal and are not likely to lead to collective properties such as photoconductivity and J-aggregate bands. The dimer provides the closest approach of metal atoms in the crystal with Zn-Zn distance being 5.1 Å.

Fig. 5 shows the UV-visible absorption spectrum of suspensions of the Zn/Sn nanosheets and for comparison the spectrum of the Zn/Sn clovers. The red-shifted J-aggregate bands of the clovers at 459 nm and the tail to the red of the  $\alpha$  and  $\beta$  bands are absent for the nanosheets. This is expected as there are no extended slipped  $\pi$ - $\pi$  stacks observed in the crystal structure. In the case of the clovers, part of the intensity of the J-aggregate bands is due to resonance light scattering rather than light absorption. The light scattering is considerably less for the nanosheets because the resonance scattering is weak or absent and the thin sheets transmit the light without much scattering. The spectra of suspensions of the sheets and the clovers have contributions from dissolved porphyrins. The (monomeric) solution contribution is significant for the nanosheets so we also show a spectrum of the nanosheets deposited onto a glass slide. A red shift in the absorption bands is observed but the shift is smaller than for the J-aggregate band of the clovers, suggesting weaker coupling of the transition dipoles.

Fig. 6 shows atomic force microscopy (AFM) images of a 65 nm thick nanosheet (Fig. 6a,b) and plots the photocurrent through the nanosheet determined using conducting AFM (Fig. 6d,e). For the tip located at point 1 (Fig. 6b) on the gold substrate a high current (not shown) is observed with either bias of the applied tip-to-surface voltage as expected for contact with a conducting metal. At points 2 or 3 on the nanosheet (Fig. 6b), a much smaller current is detected for either bias and the current is unaltered when the nanosheet is irradiated with visible light.



**Fig. 5** UV-visible absorption spectrum of a suspension of the Zn/Sn nanosheets (red) and deposited on a glass slide, and for comparison the spectra of the constituent porphyrins in solution (dashed gray) and a spectrum of the analogous Zn/Sn clover-like structures.



**Fig. 6** Conducting AFM (a, b) and optical (c, Inset) images, height profile, and current *versus* voltage curves under visible light illumination (d) and in the dark (e). The numbered points in (b) indicate positions at which the current curves (not all shown) were measured. The voltage was swept from  $-12$  V to  $+12$  V (red line) and from  $+12$  V to  $-12$  V (black line) with a voltage step of  $0.25$  V. Topography images and current *versus* voltage curves were obtained using a Dimension 3100 Nanoscope IV in contact mode under visible light illumination and in the dark. The optical resolution was  $500$  by  $500$  pixels.

The nanosheet solid is formed from an equal proportion of electron donors (ZnTPPS) and acceptors (SnTNMePyP) with the same energy levels (redox potentials) as the Zn and Sn porphyrins (ZnTPPS, SnTNEtOHPyP) forming the photoconducting clovers. Just as in the corresponding clovers, charge transfer is likely within the solid, but the lack of extended  $\pi$ - $\pi$  stacks likely limits the formation of mobile electrons and holes and thus a photocurrent is not expected. For the corresponding Zn/Sn clovers,  $\pi$ - $\pi$  stacking is evident from the presence of J-aggregate bands, and charges are clearly mobile as the clovers are photoconductive.<sup>8</sup> In addition, differences in the position and number of intervening water molecules may also affect the mobility of charge carriers.

Even in the absence of a photocurrent, the nanosheets might still act as a light-harvesting structure due to exciton migration in the solid. Charge mobility is not required for the sheets to function as light-harvesting structures. Accordingly, we photocatalytically platinized<sup>23–26</sup> the nanosheets to form water-reducing nanocomposites and examined their ability to generate hydrogen in the presence of a sacrificial electron donor (triethanolamine).<sup>9</sup> The platinized nanosheets are shown in Fig. 7 and the hydrogen generation results are compared with those for the Zn/Sn clovers in Fig. 8.

The rate of hydrogen production by the Zn/Sn nanosheets is significantly lower than the analogous Zn/Sn clovers. The lower rate might be caused by the differences between the morphologies of the platinized nanosheets and clovers. For example, SEM images of the platinized Zn/Sn nanosheets obtained before (Fig. 7a) and after (Fig. 7b) 10 days of continuous irradiation with visible light show that the nanoscale platinum does not adhere as well to the smooth surfaces of the nanosheets as it does to the rough Zn/Sn clovers.<sup>9</sup> Although an adequate amount of platinum is available as a colloid to catalyze the conversion of reduced methylviologen and protons to  $H_2$ , direct electron transfer from the nanosheets to the platinum catalyst is limited

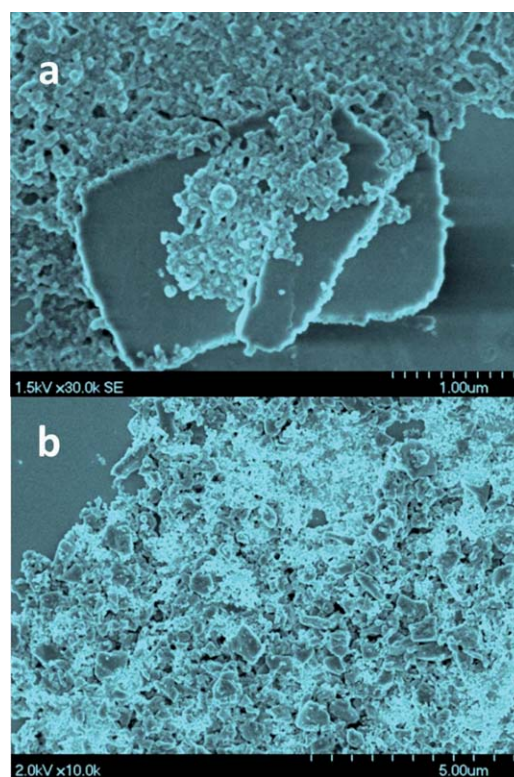


**Fig. 7** The platinized Zn/Sn nanosheets before (a) and after (b) hydrogen generation for 10 days with continuous irradiation. The nanosheets are the darker colored material. Most of the lighter platinum nanomaterial is not associated with the nanosheets. The sheets are broken into smaller pieces in (b) probably as a result of stirring.

for the nanosheets, likely reducing the rate of  $H_2$  production. Possible differences in surface areas of the nanosheets and clovers may also contribute to the lower hydrogen production rate observed for the nanosheets *versus* the clovers. Another factor is the low charge mobility in the nanosheets compared to the photoconductive clovers. Without electrons generated internally being able to migrate to the surface of the nanosheets

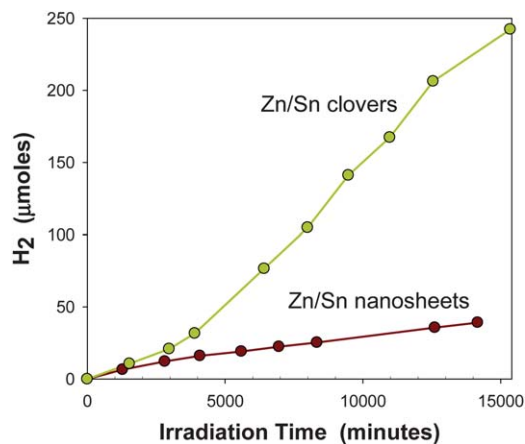


**Fig. 8** Hydrogen generated by platinized Zn/Sn nanosheets or Zn/Sn clovers as a function of irradiation time with visible light from an incandescent lamp ( $0.1$  W  $cm^{-2}$ ). Triethanolamine was used as a sacrificial electron donor and methylviologen as an electron relay molecule.

for transfer to methylviologen or directly to the Pt catalyst, less hydrogen can be produced. Because higher crystallinity usually increases charge mobility, the lower charge mobility of the nanosheets would not have been anticipated without knowledge of the detailed spatial arrangement of porphyrin molecules in the crystal that shows the absence of extended  $\pi$ - $\pi$  stacking.

## Conclusions

This first crystal structure of a cooperative binary ionic solid enriches our understanding of this new class of optoelectronic materials. The structure confirms that the interactions of the ionic substituents alone neutralize charge and thus the ratio of molecular charges determines the relative proportion of the porphyrin anions and cations in the solid. This was also the case for the porphyrin clovers.<sup>8,9</sup> The structure is similar to crystal structures of other single ionic porphyrins in that it contains many water molecules. The crystal structure also permits the rationalization of the lack of photoconductivity, the absence of J-aggregate bands in the optical spectra of the nanosheets, and their lower H<sub>2</sub> generation rates. Comparison of the crystal structure of the nanosheets with future crystal structures of other cooperative binary ionic solids will greatly aid in correlating structural features with optoelectronic and catalytic properties and aid in the design and optimization of CBI materials for specific applications.

## Acknowledgements

CJM is the recipient of a Marie Curie Fellowship from the Fundação para a Ciência e a Tecnologia, Portugal and the Marie Curie Action Cofund. Research supported by the United States Department of Energy, Office of Basic Energy Sciences, Division of Materials Sciences and Engineering. The Advanced Light Source is supported by the Director, Office of Science, Office of Basic Energy Sciences, of the U.S. Department of Energy under Contract No. DE-AC02-05CH11231. Sandia National Laboratories is a multi-program laboratory managed and operated by Sandia Corporation, a wholly owned subsidiary of Lockheed Martin Corporation, for the U.S. Department of Energy's National Nuclear Security Administration under contract DE-AC04-94AL85000.

## References

- 1 *Organic Photovoltaics: Mechanisms, Materials, and Devices*, ed. S.-S. Sun and N. S. Sariciftci, CRC Press, Boca Raton, FL, 2005.

- 2 *Introduction to Organic Electronic and Optoelectronic Materials and Devices*, ed. S.-S. Sun and L. R. Dalton, CRC Press, Boca Raton, FL, 2008.
- 3 K. Kalyanasundaram and M. Grätzel, *Coord. Chem. Rev.*, 1998, **177**, 347.
- 4 H. Hoppe and N. S. Sariciftci, *J. Mater. Res.*, 2004, **19**, 1924–1945.
- 5 *Organic Photovoltaics: Materials, Device Physics, and Manufacturing Technologies*, ed. C. J. Brabec, V. Dyakonov and U. Scherf, Wiley-VCH, 2008.
- 6 *Organic Electronics: Materials, Processing, Devices and Applications*, ed. F. So, CRC Press, Boca Raton, FL, 2009.
- 7 Z. Wang, C. J. Medforth and J. A. Shelnutt, *J. Am. Chem. Soc.*, 2004, **126**, 15954–15995.
- 8 K. E. Martin, Z. Wang, T. Busani, R. M. Garcia, Z. Chen, Y. Jiang, Y. Song, J. L. Jacobsen, T. T. Vu, N. E. Schore, B. S. Swartzentruber, C. J. Medforth and J. A. Shelnutt, *J. Am. Chem. Soc.*, 2010, **132**, 8194–8201.
- 9 Y. Tian, K. E. Martin, J. Y.-T. Shelnutt, L. Evans, T. Busani, J. E. Miller, C. J. Medforth and J. A. Shelnutt, *Chem. Commun.*, 2011, **47**, 6069–6071.
- 10 C. J. Medforth and J. A. Shelnutt, in *Handbook of Porphyrin Science*, ed. K. M. Kadish, K. M. Smith and R. Guilard, World Scientific Publishing, Hackensack, NJ, 2011, vol. 11, pp. 181–222.
- 11 C. J. Medforth, Z. Wang, K. E. Martin, Y. Song, J. L. Jacobsen and J. A. Shelnutt, *Chem. Commun.*, 2009, 7261–7277.
- 12 J. A. Shelnutt and C. J. Medforth, in *Organic Nanomaterials*, ed. G. Bottari and T. Torres, Wiley, 2011, in press.
- 13 W. M. Hikal and H. J. Harmon, *Polyhedron*, 2009, **28**, 113–120.
- 14 W. Jentzen, J. G. Ma and J. A. Shelnutt, *Biophys. J.*, 1998, **74**, 753–763.
- 15 W. Jentzen, X. Z. Song and J. A. Shelnutt, *J. Phys. Chem. B*, 1997, **101**, 1684–1699.
- 16 L. Di Costanzo, S. Geremia, L. Randaccio, R. Purrello, R. Lauceri, D. Sciotto, F. G. Gulino and V. Povone, *Angew. Chem., Int. Ed.*, 2001, **40**, 4245–4247.
- 17 F. C. F. Korber, J. R. L. Smith, S. Prince, P. Rizkallah, C. D. Reynolds and D. R. Shawcross, *J. Chem. Soc., Dalton Trans.*, 1991, 3291–3294.
- 18 J. F. Kirner, J. Garofalo Jr. and W. R. Scheidt, *Inorg. Nucl. Chem. Lett.*, 1975, **11**, 107–112.
- 19 R. De Zorzi, N. Guidolin, L. Randaccio, R. Purrello and S. Geremia, *J. Am. Chem. Soc.*, 2009, **131**, 2487–2489.
- 20 R. De Zorzi, B. Dubessy, J.-C. Mulatier, S. Geremia, L. Randaccio and J.-P. Dutasta, *J. Org. Chem.*, 2007, **72**, 4528–4531.
- 21 S. Geremia, L. Di Costanzo, G. Nardin, L. Randaccio, R. Purrello, D. Sciotto, R. Lauceri and F. Pichierrì, *Inorg. Chem.*, 2004, **43**, 7579–7581.
- 22 H. Kanemitsu, R. Harada and S. Ogo, *Chem. Commun.*, 2010, **46**, 3083–3085.
- 23 Z. Wang, K. J. Ho, C. J. Medforth and J. A. Shelnutt, *Adv. Mater.*, 2006, **18**, 2557–2560.
- 24 Z. Wang, Z. Li, C. J. Medforth and J. A. Shelnutt, *J. Am. Chem. Soc.*, 2007, **129**, 2440–2441.
- 25 Z. Wang, L. E. Lybarger, W. Wang, C. J. Medforth, J. E. Miller and J. A. Shelnutt, *Nanotechnology*, 2008, **19**, 395604.
- 26 Z. Wang, C. J. Medforth and J. A. Shelnutt, *J. Am. Chem. Soc.*, 2004, **126**, 16720–16721.